

Specialized Decision Surface and Disentangled Feature for Weakly-Supervised Polyphonic Sound Event Detection

Liwei Lin^{1,2}, Xiangdong Wang¹, Hong Liu¹, and Yueliang Qian¹

Abstract—In this paper, a special decision surface for the weakly-supervised sound event detection (SED) and a disentangled feature (DF) for the multi-label problem in polyphonic SED are proposed. We approach SED as a multiple instance learning (MIL) problem and utilize a neural network framework with a pooling module to solve it. General MIL approaches include two kinds: the instance-level approaches and embedding-level approaches. We present a method of generating instance-level probabilities for the embedding level approaches which tend to perform better than the instance-level approaches in terms of bag-level classification but can not provide instance-level probabilities in current approaches. Moreover, we further propose a specialized decision surface (SDS) for the embedding-level attention pooling. We analyze and explained why an embedding-level attention module with SDS is better than other typical pooling modules from the perspective of the high-level feature space. As for the problem of the unbalanced dataset and the co-occurrence of multiple categories in the polyphonic event detection task, we propose a DF to reduce interference among categories, which optimizes the high-level feature space by disentangling it based on class-wise identifiable information and obtaining multiple different subspaces. Experiments on the dataset of DCASE 2018 Task 4 show that the proposed SDS and DF significantly improve the detection performance of the embedding-level MIL approach with an attention pooling module and outperform the first place system in the challenge by 6.6 percentage points.

Index Terms—Sound event detection, machine learning, weakly-supervised learning, attention pooling.

I. INTRODUCTION

_SOUND event detection (SED) is the task to detect and recognize individual sound sources in realistic soundscapes. It is required to recognize not only the presence of each event category in a sound source but also the start and end boundaries of each existing event. Since sounds carry a large amount of information about our everyday environment, SED supports many applications in everyday life, such as noise monitoring for smart cities [1], bioacoustic species and migration monitoring [2], [3], surveillance [4], healthcare [5], and large-scale multimedia indexing [6].

Polyphonic SED is often approached as a multi-label classification problem. Ideally, each event category to detect is modeled equivalently, regardless of the effect of co-occurrence of multiple events on each other. Moreover, a large amount of

clean and balanced data with strong annotations (annotations with detailed timestamps for all event occurrences) is required for the model to train. However, in real life, the problem can be more complex. For example, noises out of the domain occurring in the audio recording increase the difficulty of the detection, unbalanced dataset and the co-occurrence of different events interfere with the detection of each other. Besides, it costs a lot to obtain large-scale strongly-annotated training data. Therefore, in this paper, noticing the difficulty to obtain large-scale strongly-annotated data and the problem caused by the co-occurrence of different events in the unbalanced dataset, we mainly focus on weakly-supervised SED and try to mitigate the impact of multi-event co-occurrence on the weakly-supervised SED system.

Weakly-supervised SED utilizes weak annotations, which only indicate the presence of event categories, rather than strong annotations during training. In this paper, we approach weakly-supervised SED as a multiple instance learning (MIL) problem and utilize a neural network framework with a pooling module to solve it. The MIL approaches provide strategies to decide the bag-level probability of a bag depending on all the instances in the bag. The pooling modules, such as global max pooling (GMP) [7], global average pooling (GAP) [8], global weighted rank pooling (GWRP) [9], [10], noisy-or pooling [11] and attention pooling (ATP) [12], provide more detailed methods to integrate the instance-level probabilities into a bag-level probability or the instance-level feature representations into a bag-level contextual representation. The MIL approaches are distinguished as the instance-level approach and the embedding-level approach [12]. Since Ilse et al. [12] point out that the embedding-level approach is superior to the instance-level approach in terms of bag-level classification and most of the current work on weakly-supervised SED mainly focus on the instance-level approaches, we illustrate and demonstrate the effectiveness of the embedding-level approach on weakly-supervised SED. Since the embedding-level approach does not provide the instance-level probabilities, we propose a shared decision surface for it to generate the instance-level probabilities. We argue that the classifier learning from the bag-level contextual representation forms a shared decision surface of both the bag-level contextual representation and the instance-level high-level feature representations, for which the instance-level probabilities could be obtained by passing the instance-level high-level feature representations through the same classifier directly. Then we are able to compare the embedding-level performances of different MIL approaches

¹Beijing Key Laboratory of Mobile Computing and Pervasive Device, Institute of Computing Technology, Chinese Academy of Sciences, Beijing, China

²University of Chinese Academy of Sciences, Beijing, China

cooperating with different pooling modules.

Furthermore, we propose a specialized decision surface to make better instance-level predictions than the shared decision surface for the embedding-level ATP. Compared to other pooling modules without trainable parameters such as GAP and GMP, ATP is more flexible and potential to learn detailed instance-level information. We argue that the trainable parameters in the embedding-level ATP imply a better instance-level decision surface, namely the proposed specialized decision surface, for the embedding-level ATP to give the instance-level probabilities. We demonstrate that the embedding-level approach with the shared decision surface tends to perform better than the instance-level approach and the proposed specialized decision surface is more conducive to instance-level classification than the shared decision surface on the experimental dataset.

Besides, to mitigate the impact of multi-event co-occurrence of the unbalanced dataset on the proposed weakly-supervised polyphonic SED system, we also propose a disentangled feature, which re-models the high-level feature space so that the feature subspace of a certain category differs from other categories without pre-training. Since the disentangled feature re-models both the instance-level and the bag-level high-level feature space, it aims at the multi-label problem of both the weak labels and the overlapping sound events of the strong labels for polyphonic SED. The volume of these disentangled feature subspaces depends on the number of available clips containing strong class-wise identifiable information with little interference from other categories. In virtue of the introduction of more class-wise prior information as well as network redundancy weight reduction, the disentangled feature is able to improve the performance of the polyphonic SED system.

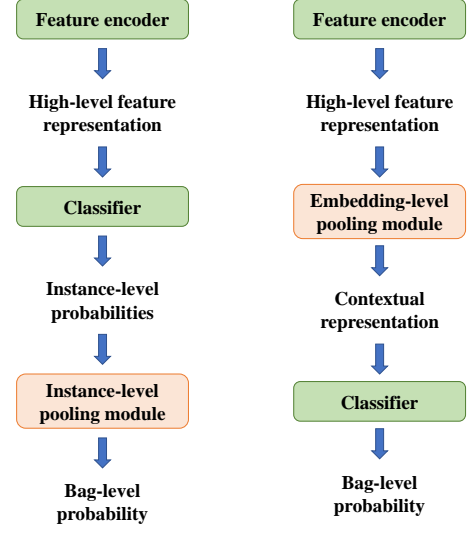
Our experiments show that the embedding-level ATP with specialized decision surface and disentangled feature outperforms other pooling modules as well as simple embedding-level ATP. Detailed analysis of the high-level feature space in the experiment also supports our hypothesis.

The rest of this paper is organized as follows. We introduce related work about weakly-supervised polyphonic SED in Section II, describe in detail the MIL framework with different pooling modules in Section III, introduce the proposed methods in Section IV, describe the dataset and configuration of our experiments in Section V, analyze the results of experiments in Section VI and draw conclusions in Section VII.

II. RELATED WORK

A. Multiple instance learning

Weakly supervised learning is often approached as an MIL problem [13], [14]. It is especially common in medical image [15], [16] and semantic segmentation [17], [18]. The excellent performance of neural networks in various fields promotes the combination of the MIL framework and neural networks for weakly supervised learning [19], [20], [21], [22]. According to MIL, a bag of several instances has only bag-level annotations, in other words, does not have instance-level annotations. If there is at least one positive instance in a bag, the bag is annotated as a positive bag. Otherwise, the bag is annotated as



(a) Instance-level approach (b) Embedding-level approach

Fig. 1. The comparison of the instance-level approach and the embedding-level approach.

a negative bag. The combination of the MIL framework and neural networks focuses on how to integrate several instance-level outputs of neural networks into a bag-level output so as to enable the model to calculate loss with only clip-level annotations and carry out end-to-end learning. Since neural networks have been widely used as a general high-level feature extractor in various tasks, the MIL framework with neural networks typically comprises a neural network feature extractor which generates the high-level feature representation sequence and a pooling module such as GMP, GAP, GWRP and ATP, which integrates instance-level outputs into a bag-level output.

As mentioned in [12] and shown in Figure 1, the MIL approaches with neural network are distinguished as instance-level approaches and embedding-level approaches according to whether the pooling module involved in the MIL framework integrates instance-level probabilities into a bag-level probability or integrates instance-level high-level feature representations into a bag-level high-level feature representation. Ilse et al. [12] also point out that the embedding-level approach is superior to the instance-level approach in terms of bag-level classification and proposes an attention-based embedding-level approach, which performs the best compared to other MIL approaches.

B. Weakly-supervised sound event detection

As for weakly-supervised SED, if we treat each frame in an audio clip as an instance, then the audio clip can be regarded as a bag with clip-level annotations (without frame-level annotations of frames). If a sound event occurs in any frame of the audio clip, the clip is considered as a positive clip of the event. Otherwise, the audio clip is treated as a negative audio clip.

Since a pooling module described in the previous section is essential to an MIL framework with neural network, there are lots of previous works about MIL with different pooling

modules for weakly-supervised SED: a fully convolutional network with a GMP module [23], a joint detection-classification (JDC) model with a ATP module [24], a convolutional neural network (CNN) based model with a GAP module [25], a gated convolutional recurrent neural network (CRNN) with a global softmax pooling (GSP) module [26] and a joint separation-classification (JSC) model with a GWRP module [10]. Especially, McFee et al. [27] explore the effects of different pooling modules such as GAP, GMP and GSP and propose an adaptive pooling module. Wang et al. [28] offer a comparison of several pooling modules including GAP, GMP, GSP and ATP.

However, all these work described above just considers the instance-level approaches. To explore the effects of different pooling modules cooperating with both of instance-level and embedding-level approaches on SED, we carry out a series experiments and find that the embedding-level approach tends to perform better.

C. Polyphonic sound event detection

Since multiple event categories tend to occur in co-occurrence in an audio clip, a SED system is also termed as a polyphonic SED system [29], [30], [31]. Recently, neural networks such as recurrent neural network (RNN) [32] and CRNN [31] show a significant effect on polyphonic SED. Commonly, these methods model each event category equally. When designing models, they make all the categories share the same feature encoder. However, in realistic sound environment, multiple events overlapping in the unbalanced dataset, such as “Dishes” and “Frying”, would interfere with the recognition of each other, especially when the numbers of clips of some event categories are relatively small and thereby less identifiable information about these event categories can be available. During training, the feature encoder tends to fit better for some event categories with more identifiable information than those with little identifiable information. To tackle this problem, Imoto et al. [33] proposes a neural-network-based SED with graph Laplacian regularization based on the co-occurrence of sound events. We also focus on this problem and try to take advantage of more prior information about the data distribution to optimize the high-level feature space of the feature encoder, thereby making more accurate classification and detection for overlapping events.

III. MIL FOR WEAKLY-SUPERVISED POLYPHONIC SED

In this section, we describe in detail the MIL framework for weakly-supervised polyphonic SED. 8 common pooling modules including 4 instance-level pooling modules and 4 embedding-level pooling modules are introduced.

A. The MIL framework

For weakly-supervised polyphonic SED, since multiple different events might appear in co-occurrence in the same audio clip, we consider each event category separately when approaching SED as an MIL problem. Assuming that there are C event categories to detect, then for event category c , we

treat an audio clip as a positive audio clip if the audio clip contains event category c . Otherwise, the audio clip is treated as a negative audio clip. Let $\mathbf{x} = \{\mathbf{x}_1, \mathbf{x}_2, \dots, \mathbf{x}_T\}$ be the high-level feature representations of the audio clip generated by the feature encoder and $\mathbf{y} = \{y_1, y_2, \dots, y_C\}$ ($y_c \in \{0, 1\}$) be the groundtruths, where C is the number of categories.

For the instance-level approach, for each event category c , the high-level feature representations are passed into the classifier to generate frame-level probabilities $\hat{p}(y_c | \mathbf{x}_1), \hat{p}(y_c | \mathbf{x}_2), \dots, \hat{p}(y_c | \mathbf{x}_t), \dots, \hat{p}(y_c | \mathbf{x}_T)$. Then the instance-level pooling module aggregates frame-level probabilities into a clip-level probability:

$$\hat{P}(y_c | \mathbf{x}) = \text{POOLING}\{\hat{p}(y_c | \mathbf{x}_1), \dots, \hat{p}(y_c | \mathbf{x}_T)\}. \quad (1)$$

When making predictions, assuming that α is a threshold for clip-level prediction and γ is a threshold for frame-level prediction. Then the clip-level prediction is:

$$\phi_c(\mathbf{x}) = \begin{cases} 1, & \hat{P}(1 | \mathbf{x}) \geq \alpha \\ 0, & \text{otherwise} \end{cases}, \quad (2)$$

where $\hat{P}(1 | \mathbf{x})$ denotes the probability that the clip is predicted to be positive. The the frame-level prediction at time t is:

$$\varphi_c(\mathbf{x}, t) = \begin{cases} 1, & \hat{p}(1 | \mathbf{x}_t) \cdot \phi_c(\mathbf{x}) \geq \gamma \\ 0, & \text{otherwise} \end{cases}, \quad (3)$$

where $\hat{p}(1 | \mathbf{x}_t)$ denotes the probability that the t^{th} frame is predicted to be positive. Without loss of generality, we set $\alpha = 0.5$ and $\gamma = 0.5$ in our experiments.

For the embedding-level approach, the embedding-level pooling module directly aggregates all the high-level feature representations into a contextual representation \mathbf{h}_c :

$$\mathbf{h}_c = \text{POOLING}(\mathbf{x}_1, \mathbf{x}_2, \dots, \mathbf{x}_T). \quad (4)$$

Then the clip-level probability can be obtained by passing the contextual representation into the classifier:

$$\hat{P}(y_c | \mathbf{x}) = \hat{P}(y_c | \mathbf{h}_c) = G_c(\mathbf{h}_c), \quad (5)$$

where G_c is the classifier of \mathbf{h}_c to generate the clip-level probability. Therefore, the clip-level prediction for the embedding-level approach can be obtained according to Equation 2 and 5.

B. Instance-level pooling modules

We introduce 4 typical pooling modules for the instance-level MIL, namely GMP, GAP, GSP, and ATP. These 4 instance-level pooling modules are commonly used in weakly SED, such as GMP in [23], GAP in [25], GSP in [26], [34] and ATP in [24].

For GMP, the clip-level probability only depends on the maximum probability of all the frame-level probabilities of an audio clip:

$$\hat{P}(y_c | \mathbf{x}) = \max_t \hat{p}(y_c | \mathbf{x}_t). \quad (6)$$

For GAP, the clip-level probability relates to all the frame-level probabilities of an audio clip. More specifically, it takes the

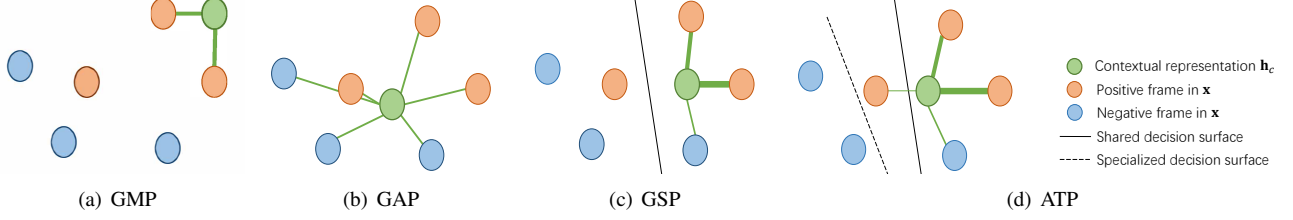


Fig. 2. A sketch of the relation of \mathbf{h}_c and \mathbf{x} of a positive audio clip in the 2-dimension feature space for event category c .

average value of all the frame-level probabilities as clip-level probabilities:

$$\hat{P}(y_c | \mathbf{x}) = \frac{1}{T} \sum_t \hat{p}(y_c | \mathbf{x}_t). \quad (7)$$

Obviously, since $\hat{P}(y_c | \mathbf{x})$ only relates to the s^{th} high-level feature representation \mathbf{x}_s ($s = \text{argmax } \hat{p}(y_c | \mathbf{x}_t)$), GMP only updates a limited number of weights of the neural network for each clip. On the other hand, although GAP considers all the high-level feature representations when updating the neural network, it focuses on each frame equally, ignoring the different degrees how much a frame contributes to the audio clip. Then a weighted pooling is proposed to fix this defect:

$$\hat{P}(y_c | \mathbf{x}) = \sum_t a_{ct} \cdot \hat{p}(y_c | \mathbf{x}_t), \quad (8)$$

where a_{ct} denotes the contribution of the t^{th} frame to an audio clip for event category c .

GSP and ATP are two examples of such weighted pooling modules, where GSP connects the contribution of frames with frame-level probabilities:

$$a_{ct} = \frac{\exp(\psi(\hat{p}(y_c | \mathbf{x}_t)))}{\sum_k \exp(\psi(\hat{p}(y_c | \mathbf{x}_k))), \quad (9)}$$

where ψ is a function to scale $\hat{p}(y_c | \mathbf{x}_t)$ appropriately.

Different from GSP, ATP offers an independent detector to generate the contribution of frames. This independent detector is learnable and in this paper, we give a common form of such an independent detector:

$$a_{ct} = \frac{\exp(\mathbf{w}_c^\top \mathbf{x}_t / d)}{\sum_k \exp(\mathbf{w}_c^\top \mathbf{x}_k / d)}, \quad (10)$$

where \mathbf{w}_c are learnable parameters of the given independent detector and d is a scaling factor to avoid too-large value of $\mathbf{w}_c^\top \mathbf{x}_t$. The value of d is generally consistent with the dimensions of \mathbf{x}_t .

C. Embedding-level pooling modules

We describe how the 4 pooling modules discussed above cooperate with the embedding-level MIL approach. In fact, though the embedding-level MIL approach is introduced and claimed to be superior to the instance-level MIL approach in [12], its application in SED is rare.

Different from the instance-level pooling modules, the embedding-level pooling modules work by integrating high-level feature representations \mathbf{x} instead of frame-level probabilities $\hat{p}(y_c | \mathbf{x}_t)$ as described in Section III-A.

For GMP, assuming that the contextual representation $\mathbf{h}_c = \{h_{c1}, h_{c2}, \dots, h_{cZ}\}$ is an Z -dimensional vector and x_{tz} is the z^{th} component of \mathbf{x}_t , then the z^{th} component of the contextual representation \mathbf{h}_c is

$$h_{cz} = \max \{x_{1z}, x_{2z}, \dots, x_{tz}, \dots, x_{Tz}\}. \quad (11)$$

For GAP, the contextual representation \mathbf{h}_c is:

$$\mathbf{h}_c = \frac{1}{T} \sum_t \mathbf{x}_t. \quad (12)$$

For GSP and ATP, the contextual representation \mathbf{h}_c is:

$$\mathbf{h}_c = \sum_t a_{ct} \cdot \mathbf{x}_t. \quad (13)$$

Similar to instance-level pooling modules, a_{ct} , the contribution of \mathbf{x}_t to an audio clip for event category c is attained by Equation 9 for GSP and by Equation 10 for ATP.

IV. METHODS

In this section, we propose how to generate frame-level probabilities for the embedding-level approach and introduce the proposed specialized decision surface (SDS) and disentangled feature (DF).

A. Shared decision surface

Since there are no frame-level probabilities generated during learning, we propose that the clip-level contextual representation and frame-level high-level feature representations can share the same classifier, despite the fact that the classifier is simply utilized for classification of the contextual representation during training.

We argue that not only the model learns the decision surface (the classifier) explicitly for \mathbf{h}_c but also learn a latent decision surface for \mathbf{x} . Since this latent decision surface can not be obtained directly, we consider it to be close to the decision surface of \mathbf{h}_c .

As shown in Figure 2, to simplify the analysis, we assume that the high-level feature space is a 2-dimension space and sketch the relation of \mathbf{h}_c and \mathbf{x} in this 2-dimension feature space for event category c . The green circles represent \mathbf{h}_c , the orange circles represent positive frames in \mathbf{x} and the blue circles represent negative frames in \mathbf{x} . We connect \mathbf{h}_c and \mathbf{x} in the following way: draw a line between \mathbf{h}_c and a frame in \mathbf{x} if there is a connection between them and let the thickness of the line corresponding to the frame indicates the strength of the connection.

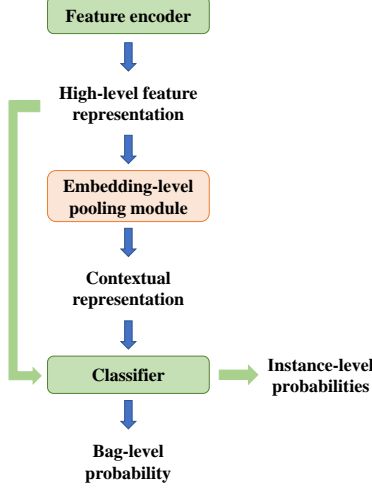


Fig. 3. The instance-level probabilities for the embedding-level approach.

We assume that the decision surface is fixed, and explore how the feature encoder tends to form a high-level feature space to fit the decision surface. The relative position of the high-level feature representation of each frame to the decision surface changes constantly with the formation of the feature space. During training, the green circle of a positive audio clip tends to move toward the positive side of the decision surface, which implies that those circles connected with the green circles move with the green circle together. On the contrary, those circles connected with the green circle in a negative audio clip tends to move toward the negative side of the decision surface.

If circles (except green circles) with such a connection are considered to be positive and the strength of the connection is related to the confidence that it is considered positive, then the movement in a positive audio clip carries these (both true-positive and false-positive) circles toward the positive side of the decision surface. Since there is no true-positive circle in a negative audio clip, the movement in this circumstance actually carries false-positive circles toward the negative side of the decision surface. Attribute to these movements, positive (true-positive) frames and negative (false-positive) frames are able to gradually separate into two clusters and the decision surface of the contextual representations is close to the boundary of such two clusters, in other words, suitable for coarse frame-level classification, for which we regard it as a shared decision surface.

According to Equation 11, \mathbf{h}_c in GMP only relates to two frames in an audio clip, the value of the high-level feature representation of which in one dimension is the largest of all frames, as shown in Figure 2(a). Thus the movements in GMP affect fewer frames in a negative audio clip but make fewer mistakes in a positive audio clip (carry fewer false-positive frames toward the positive side of the decision surface). Similarly, \mathbf{h}_c in GAP relates to all the frames and focuses on them equally as shown in Figure 2(b), for which it affects all the frames in a negative audio clip but makes more mistakes in a positive audio clip. For GSP, according to Equation 9 and 13, the strength of the connection a_{ct} depends on $\hat{p}(y_c | \mathbf{x}_t)$. Since we consider that \mathbf{x}_t and \mathbf{h}_c share the same decision surface,

the strength of the connection a_{ct} in GSP exactly depends on this shared decision surface. Therefore, the strength of the connection between \mathbf{x}_t and \mathbf{h}_c exactly depends on how much the model considers it as a positive frame. As shown in Figure 2(c), where the black solid line represents the decision surface mentioned above, if we ignore some of the relatively weak connection, those green lines between \mathbf{h}_c and \mathbf{x}_t lying on the negative side of the decision surface can be neglected. Hence, GSP pursues a trade-off between affecting more frames in a negative audio clip and making fewer mistakes in a positive audio clip.

Therefore, for the embedding-level approach, for GMP, GAP and GSP, as shown in Figure 3, we pass the frame-level high-level feature representation \mathbf{x}_t through clip-level classifier to get frame-level probabilities $\hat{p}(y_c | \mathbf{x}_t)$ for event c at time t . Then the frame-level prediction is:

$$\varphi_c(\mathbf{x}, t) = \begin{cases} 1, & G_c(\mathbf{x}_t) \cdot \phi_c(\mathbf{x}) \geq \gamma, \\ 0, & \text{otherwise} \end{cases}, \quad (14)$$

where G_c denotes the classifier of the contextual representation \mathbf{h}_c according to Equation 5.

B. Specialized decision surface

To explore the more accurate boundary of the two clusters mentioned above, we propose a specialized decision surface (SDS). Different from the shared decision surface, SDS is not approximately close to but exactly the boundary of the two clusters so that SDS is able to provide more accurate frame-level detection.

Actually, for GMP and GAP, SDS does not present in an explicit way. Intuitively, they do not provide an explicit way to separate these two clusters. However, as for GSP, according to Equation 8 and 9, the forming of the two clusters depends on a_{ct} relating to the shared decision surface G_c , so that SDS of GSP is coincident with the shared decision surface of GSP.

When it comes to ATP, according to Equation 10, the strength of the connection a_{ct} depends on the independent detector discussed in Section III-A instead of the shared decision surface G_c as shown in Figure 2(d). Therefore, free parameters \mathbf{w}_c in the independent detector (dotted line in Figure 2(d)) determine how to chose frames to move with the contextual representation together and gradually separate these frames from the rest. Although these movements try to promote the two clusters to distribute separately on opposite sides of the shared decision surface, the SDS utilized directly to select and separate the two clusters can better match the boundaries of the two clusters.

Therefore, the implement of SDS for the embedding-level attention pooling is based on a frame-level classifier S_c : the combination of the independent detector utilized to generate a_{ct} and an activation layer employed to generate probabilities.

Then the frame-level prediction for event c at time t is:

$$\varphi_c(\mathbf{x}, t) = \begin{cases} 1, & S_c(\mathbf{x}_t) \cdot \phi_c(\mathbf{x}) \geq \gamma, \\ 0, & \text{otherwise} \end{cases}, \quad (15)$$

$$S_c(\mathbf{x}_t) = \sigma(\mathbf{w}_c^\top \mathbf{x}_t), \quad (16)$$

where \mathbf{w}_c are free parameters of the independent detector and σ is an activation function to generate probabilities. We take Sigmoid as this activation function in our work.

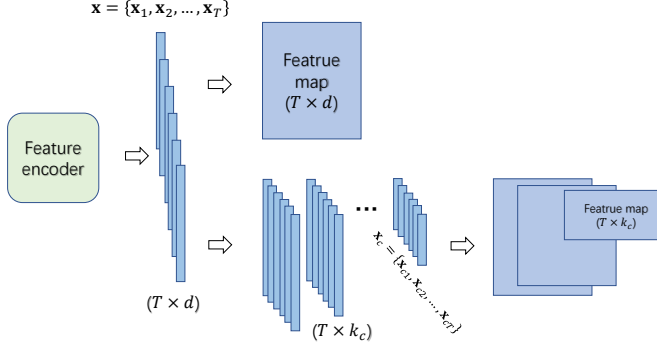


Fig. 4. The comparison of general feature (top) and disentangled feature (bottom).

C. Disentangled feature

For all the MIL approaches described above, the general feature encoder generates the high-level feature representations of all the categories from the same feature space. However, for multi-label classification, when a certain category often appears in co-occurrence with other categories, this approach makes it difficult to differentiate every single category. In other words, the forming of the high-level feature subspace of the event categories with insufficient identifiable information given in the training set will be largely disturbed by those categories appearing in co-occurrence with them. This effect will be exacerbated when the number of clips with much identifiable information of certain categories in the unbalanced set is particularly small.

To mitigate this effect, we propose DF to re-model multiple feature subspaces for multiple categories. In this way, every category shares a different part of the feature encoder instead of the whole feature encoder and is allocated in advance a feature subspace of the high-level feature space generated by the feature encoder according to its priori information.

Assuming that χ^d ($\mathbf{x} \in \chi^d$) is a d -dimensional space generated by the feature encoder and $\mathbf{B} = \{\mathbf{b}_1, \mathbf{b}_2, \dots, \mathbf{b}_d\}$ is a basis of χ^d . We define χ_c , a subspace of χ^d , as the feature space of event category c . We produce χ_c by selecting specific base vectors from \mathbf{B} and the basis of χ_c is

$$\mathbf{B}_c = \{\mathbf{b}_1, \mathbf{b}_2, \dots, \mathbf{b}_{k_c}\}, \quad (17)$$

where $\mathbf{k} = \{k_1, k_2, \dots, k_C\}$ ($0 < k_c \leq d$) relates to the volume of χ_c .

In this way, the diversity of elements in \mathbf{k} leads to the feature space of each category being remodeled into a disentangled feature space that is different from those of the other categories. For two categories i and j , the larger the absolute value of the difference between k_i and k_j is, the more different their feature space will be. The difference of feature spaces results in the diversity of decision surfaces among different categories without pre-training. In the extreme case with $k_1 = k_2 = \dots = k_C = d$, all subspaces are equal to χ^d so that the disentangled feature degenerates to general feature.

Meanwhile, if a clip contains more categories, we argue that for each of these categories, the clip contains more interference from other categories. We argue that the volume of χ_c is

determined by the number of available clips containing little interference. This is because that for category c , the larger the proportion of the clips containing little interference from other event categories is, the more the class-wise identifiable information needs to be learned, which requires the larger volume of the feature space. In contrast, the smaller the proportion of these clips is, the smaller volume of the feature space is required to prevent overfitting. For this reason, k_c increases as the proportion of these clips of category c increases.

Considering that too-small k_c severely cut into the ability of the model to recognize category c , we utilize a constant factor m ($0 \leq m \leq 1$) to tackle this effect, then,

$$k_c = \lceil ((1 - m) \cdot f_c + m) \cdot d \rceil, \quad (18)$$

where f_c ($0 \leq f_c \leq 1$) relates to the number of clips containing little interference in the training set. As m increases to 1, DF degrades into the general feature.

We quantify the level of interference according to the principle that the more categories a clip covers, the more interference the other categories cause to any one of them, then,

$$f_c = \sum_{i=1}^C \frac{r_i \cdot N_{ci}}{R}, \quad (19)$$

$$R = \max_c \sum_{i=1}^C r_i \cdot N_{ci}. \quad (20)$$

Here, N_{ci} denotes the number of clips containing i categories including category c in the training set and r_i is corresponding constant coefficient implying the importance of these clips. We argue that the less interference the other categories cause to any one of them in a clip, the more important the clip is, for which we determine r_i as:

$$r_i = \frac{1}{i} (1 \leq i \leq C). \quad (21)$$

We can also just consider those clips containing the least interference, then,

$$r_i = \begin{cases} 1, & i = 1 \\ 0, & \text{otherwise} \end{cases}. \quad (22)$$

To simplify training, we take an orthogonal basis $\mathbf{B}' = \{\mathbf{e}_1, \mathbf{e}_2, \dots, \mathbf{e}_d\}$ where the element of \mathbf{e}_i in the i^{th} dimension is 1 for χ^d . Then the k_c basis vectors are related to k_c dimensions of \mathbf{x}_t . As shown in Figure 4, we easily get a ladder-shape group of disentangled feature maps from feature encoder for a clip.

Combining disentangled feature $\mathbf{x}_c = \{\mathbf{x}_{c1}, \mathbf{x}_{c2}, \dots, \mathbf{x}_{cT}\}$ and the embedding-level attention module, to generate the contextual representation of event category c , we have

$$\hat{P}(y_c | \mathbf{x}) = \hat{P}(y_c | \mathbf{x}_c) = \hat{P}(y_c | \mathbf{h}_c), \quad (23)$$

$$\mathbf{h}_c = \sum_t a_{ct} \cdot \mathbf{x}_{ct}. \quad (24)$$

Then the contribution of \mathbf{x}_{ct} to an audio clip is:

$$a_{ct} = \frac{\exp(\mathbf{w}_c^\top \mathbf{x}_{ct} / d_c)}{\sum_k \exp(\mathbf{w}_c^\top \mathbf{x}_{ck} / d_c)}, \quad (25)$$

where \mathbf{w}_c^\top are learnable parameters mentioned in Section III-B and d_c is a scaling factor consistent with the dimensions of \mathbf{x}_{ct} .

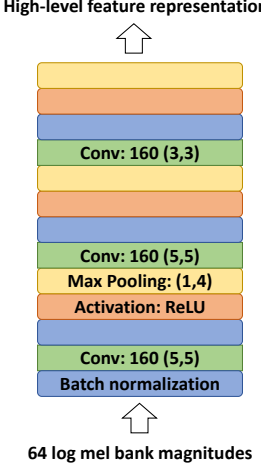


Fig. 5. The architecture of the feature encoder.

V. EXPERIMENTS

In this section, we introduce the dataset and describe in detail the model architecture, the pre-processing, and post-processing methods, the training configuration, and the evaluation measure in our experiments.

A. Dataset

We utilize the dataset from task 4 of the DCASE 2018 Challenge [35], which is a subset of AudioSet [36] by Google. The dataset consists of 10 categories of sound events from domestic environment: alarm/bell/ringing, blender, cat, dishes, dog, electric shaver/toothbrush, frying, running water, speech, and vacuum cleaner. The set contains 1578 weakly-labeled clips (2244 event occurrences) for which weak annotations have been verified and cross-checked, 14412 unlabeled in domain clips, 39999 unlabeled out-of-domain clips and 1168 clips with strong annotations. The challenge divides strong-labeled clips into two subsets: a validation set (288 clips) and an evaluation set (880 clips). In our experiments, we utilized the weakly labeled data to pre-train a clip-level classification model to tag unlabeled in domain data with weak annotations and wipe off 1001 clips with empty annotations. The clip-level classification model achieves a micro F-measure of 0.688 and a macro F-measure of 0.627 on audio tagging on the test set. Since such the feature encoder of such a model only outputs 5 frame-level high-level feature representations, the event detection performance of it is relatively poor. But it is suitable for tagging unlabeled data with weak annotations. We combine these noisy-annotated data with the original weakly-labeled training set because the weakly-labeled training set is too small to achieve stable performances of different pooling methods. Since there are also some errors occurring in annotations of some large-scale manual-labeled dataset, we argue that such a combination of data set makes sense. Consequently, the training set in our experiments embraces 14989 clips with noisy weak annotations, the characteristic of which are large scale and unbalanced distribution. Besides, there are other problems contained in this dataset, such as noisy annotations, the co-occurrence of multiple categories, overlapping sounds

TABLE I
THE DF DIMENSION AND THE WINDOW SIZE OF MEDIAN FILTERS WHEN $\beta = \frac{1}{3}$ PER CATEGORY.

Event	DF dimension		Window Size (frame)
	DF1	DFW	
Alarm bell ringing	46	31	17
Blender	22	22	42
Cat	92	43	17
Dishes	42	66	9
Dog	82	39	16
Electric shaver toothbrush	17	16	74
Frying	13	41	85
Running water	160	75	64
Speech	74	160	18
Vacuum cleaner	85	35	87

and the appearances of the sound events outside of the target categories.

B. Model architecture

The models employed in our experiments are divided into the instance-level model and the embedding-level model. As shown in Figure 1, both these two types of models comprise three modules: the feature encoder, the pooling module, and the classifier. The feature encoder is designed based on the model architecture of the baseline system of the task 4 [35]. We remove the RNN layer to make each frame-level high-level feature representation contain more identifiable information about the current frame, for which finer frame-level information is maintained. Meanwhile, the model thus depends more on the pooling module to integrate contextual information. We also remove dropout layers and increase the number of filters of CNN layers. The final feature encoder consists of 3 convolutional blocks, each of which comprises a convolutional layer, a batch normalization [37] layer, a max pooling layer (no temporal pooling), and an activation layer, as shown in Figure 5. The pooling modules including GAP, GMP, GSP and ATP are described in detail in Section III-B and Section III-C. We utilizes 1×1 convolutional layer with Sigmoid activation function as the classifier.

Different from other general pooling modules in the prediction phase, the instance-level and embedding-level ATP-SDS make frame-level prediction according to Equation 15 and Equation 16 discussed in Section IV-B.

As for DF, we experiment with two different methods for determination of the constant coefficient r_i discussed in Section IV-C: the embedding-level ATP-SDS with DFW (Equation 21) and the embedding-level ATP-SDS with DF1 (Equation 22). In addition, as mentioned in Section IV-C, since the hyper-parameter m is to avoid too-small k_c and for this dataset, each k_c is within a reasonable range, we set $m = 0$ in our experiments. Figure 6 illustrates the details of the co-occurrence of every two sound event categories on the training set and Figure 7 illustrates the condition of the embedding-level ATP-SDS with DF1. More detailed information of disentangled dimensions for each category of the DFW and DF1 methods is shown in Table I.

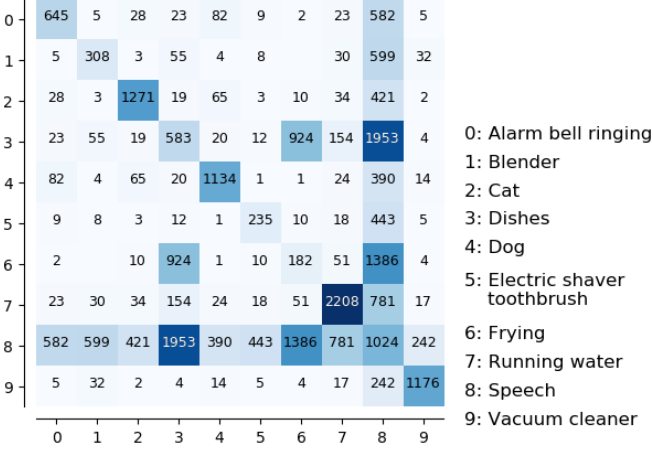


Fig. 6. The number of clips where two categories occur in co-occurrence. The diagonal represents the number of the clips containing only one category.

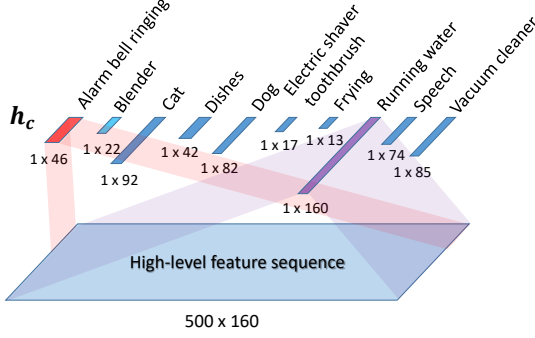


Fig. 7. A sketch of the high-level feature representations of the the embedding-level ATP-SDS with DF1.

C. Pre-processing and post-processing

The feature passed into the feature encoder employed 64 log mel-bank magnitudes (sampling rate 44.1 KHz) which are extracted from 40 ms frames with 50% overlap ($n_{FFT} = 2048$) using the librosa package [38]. All the 10-second audio clips are transformed to feature vectors with 500 frames. The threshold α (mentioned in Section III-A) of the predicted probability to determine whether an event category exists in a clip is 0.5. For frame-level prediction, all the probabilities are smoothed by a median filter with a group of adaptive window sizes. The operation of smoothing is repeated on the final frame-level prediction with a threshold $\gamma = 0.5$.

The adaptive window size of the median filter for category c is:

$$\text{win}_c = \text{duration}_c \cdot \beta, \quad (26)$$

where duration_c is the average duration of category c in the validation set. In addition, we set $\beta = \frac{1}{3}$ and shows the specific window sizes in Table I.

We argue that the average duration of each event is more like a fixed physical property. In real life, the duration of the same event is similar. Therefore, we argue the duration of the validation set is representative enough. As shown in Figure 8, we show the window sizes calculated from the validation set and the test set, and their distribution is similar. Since the

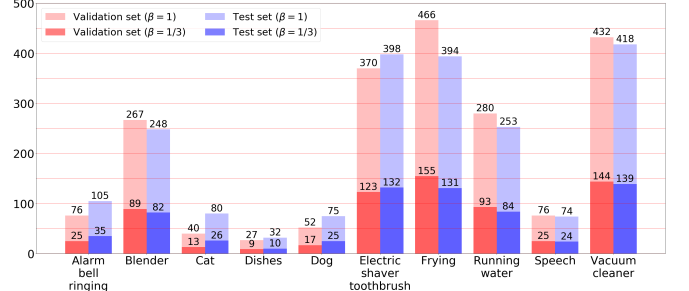


Fig. 8. The the window sizes calculated from the validation set and the test set with $\beta = 1$ and $\beta = \frac{1}{3}$ respectively.

model early stops according to the audio tagging performance of the validation set rather than the detection performance and the audio tagging performance has nothing to do with the post-processing method, the duration calculated from the validation set will not make the selected model heavily overfit the validation set. Besides, we argue that such an adaptive method tends to be superior to the method with fixed window sizes. And it is also more convenient and reliable than using empirical value to decide window sizes.

D. Training and evaluation

The neural networks are trained using the Adam optimizer [40] with learning rate of 0.0018 and mini-batch of 64 10-second patches. The learning rate is reduced by 20% per 10 epochs. We take binary cross entropy as loss function. Training stops if there is no more improvement in clip-level macro F_1 performance on the validation set within 10 epochs. The best performing model on the validation set will be retained for prediction before the training stops. All the experiments are repeated 20 times under the same parameter configuration. We fix random seeds of the CPU and the GPU, but some operations on the GPU have non-deterministic outputs. Therefore, the results of these 20 experiments were not exactly the same. We took the average of all the results as the final result. In particular, in order to compare with the performance of the first place in the challenge, we report the best results among these 20 experiments in addition. For event detection, event-based measures (macro-averaged) [41] with a 200 ms collar on onsets and a 200 ms / 20% of the events length collar on offsets are calculated over the entire test set. For audio tagging, we report the macro F_1 -score. The implementation of our methods is available online at https://github.com/Kikyo-16/Sound_event_detection.

VI. DISCUSSION

In this section, we report the results of our experiments and analyze in detail the distribution of data in the high-level feature space of models to prove our conjecture.

A. Results

We report the average results (with the 95% confidence intervals) of 20 experiments of all the models in Table II and the performance of the models with the best frame-level F_1

TABLE II
THE AVERAGE PERFORMANCE OF MODELS.

		Event detection (frame-level)			Audio tagging (clip-level)		
Model		F ₁	P	R	F ₁	P	R
Instance -level pooling	GMP	0.013 ± 0.002	0.089 ± 0.018	0.007 ± 0.001	0.565 ± 0.007	0.643 ± 0.014	0.531 ± 0.015
	GAP	0.187 ± 0.004	0.248 ± 0.007	0.172 ± 0.003	0.471 ± 0.003	0.668 ± 0.003	0.403 ± 0.004
	GSP	0.208 ± 0.006	0.266 ± 0.006	0.190 ± 0.006	0.487 ± 0.006	0.682 ± 0.007	0.412 ± 0.005
	ATP	0.260 ± 0.003	0.298 ± 0.007	0.255 ± 0.005	0.612 ± 0.010	0.743 ± 0.009	0.555 ± 0.011
	ATP-SDS	0.284 ± 0.007	0.347 ± 0.006	0.271 ± 0.007			
Embedding -level pooling	GMP	0.239 ± 0.006	0.249 ± 0.009	0.245 ± 0.006	0.626 ± 0.005	0.674 ± 0.006	0.610 ± 0.008
	GAP	0.242 ± 0.004	0.247 ± 0.006	0.265 ± 0.005	0.602 ± 0.005	0.657 ± 0.005	0.597 ± 0.007
	GSP	0.242 ± 0.004	0.243 ± 0.006	0.268 ± 0.005	0.608 ± 0.005	0.660 ± 0.006	0.603 ± 0.007
	ATP	0.253 ± 0.004	0.247 ± 0.005	0.301 ± 0.007	0.620 ± 0.005	0.665 ± 0.005	0.634 ± 0.007
	ATP-SDS	0.349 ± 0.004	0.364 ± 0.007	0.370 ± 0.003			
eATP-SDS	DFW	0.358 ± 0.004	0.365 ± 0.007	0.374 ± 0.005	0.639 ± 0.006	0.682 ± 0.006	0.624 ± 0.009
	DF1	0.359 ± 0.008	0.373 ± 0.008	0.373 ± 0.006	0.634 ± 0.006	0.679 ± 0.005	0.620 ± 0.006

TABLE III
THE PERFORMANCE OF THE MODELS WITH THE BEST FRAME-LEVEL F₁ SCORE IN 20 EXPERIMENTS.

		Event detection			Audio tagging		
Model		F ₁	P	R	F ₁	P	R
Baseline system [35]		0.141	-	-	-	-	-
The 1 st place [39]		0.324	-	-	-	-	-
Instance -level pooling	GMP	0.023	0.094	0.014	0.596	0.641	0.576
	GAP	0.202	0.271	0.186	0.482	0.670	0.410
	GSP	0.240	0.302	0.218	0.518	0.696	0.426
	ATP	0.273	0.315	0.260	0.636	0.735	0.586
	ATP-SDS	0.312	0.364	0.302			
Embedding -level pooling	GMP	0.271	0.274	0.286	0.648	0.683	0.639
	GAP	0.258	0.266	0.278	0.614	0.656	0.598
	GSP	0.252	0.245	0.279	0.628	0.667	0.616
	ATP	0.267	0.268	0.309	0.643	0.663	0.663
	ATP-SDS	0.362	0.398	0.365			
eATP-SDS	DFW	0.380	0.397	0.375	0.658	0.676	0.649
	DF1	0.390	0.402	0.402	0.650	0.684	0.632

score among these 20 experiments in Table III. As shown in Table II, the embedding-level ATP-SDS with DF1 achieves the best average frame-level F₁ score of 0.359 among all the models. The best performance of ATP-SDS with DF1 shown in Table III achieves **0.390**, outperforming the first place (**0.324**) [39] in the challenge by **6.6** percentage points. The embedding-level ATP-SDS with DFW achieves the best average clip-level F₁ score of 0.639 among all the models.

We illustrate the average results with the confidence interval of the 20 experiments in Figure 9. Since different window sizes of median filters in post-processing have a great impact on results, we show frame-level performances of all the models when window sizes are fixed with 27 and adaptive window sizes employ different β ($\beta = \frac{1}{2}$, $\beta = \frac{1}{3}$, $\beta = \frac{1}{4}$ and $\beta = \frac{1}{5}$) respectively. As shown in Figure 9, the value of β shows a significant effect on the frame-level performance of the model and the model tends to perform the best with $\beta = \frac{1}{3}$.

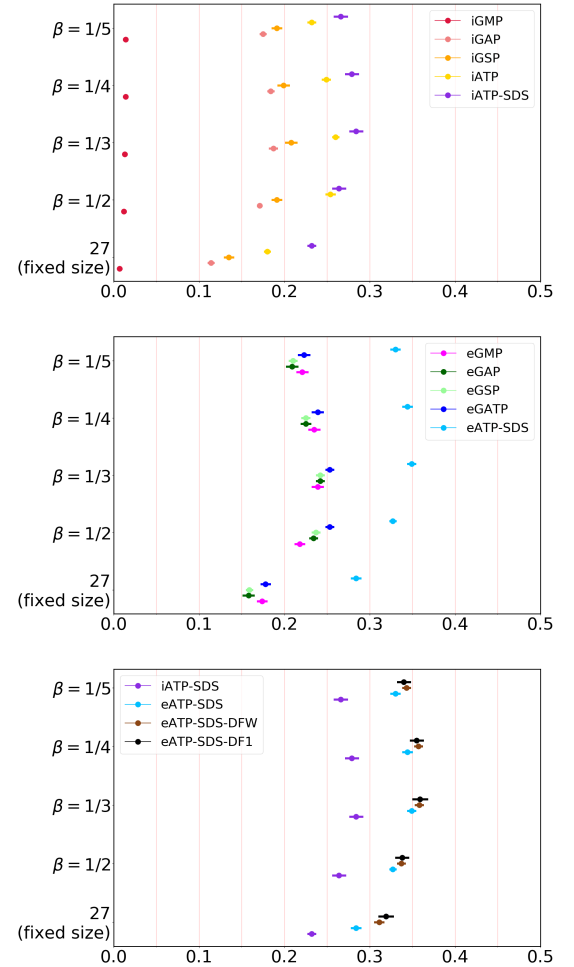


Fig. 9. The frame-level F₁ score of all 20 experiments of all the models with different window sizes of median filters. i* such as iGMP represents the instance-level model and e* such as eGMP represents the embedding-level model.

B. The performances of different pooling modules

By comparing the performances of the embedding-level models with those of the instance-level models in Table II, we

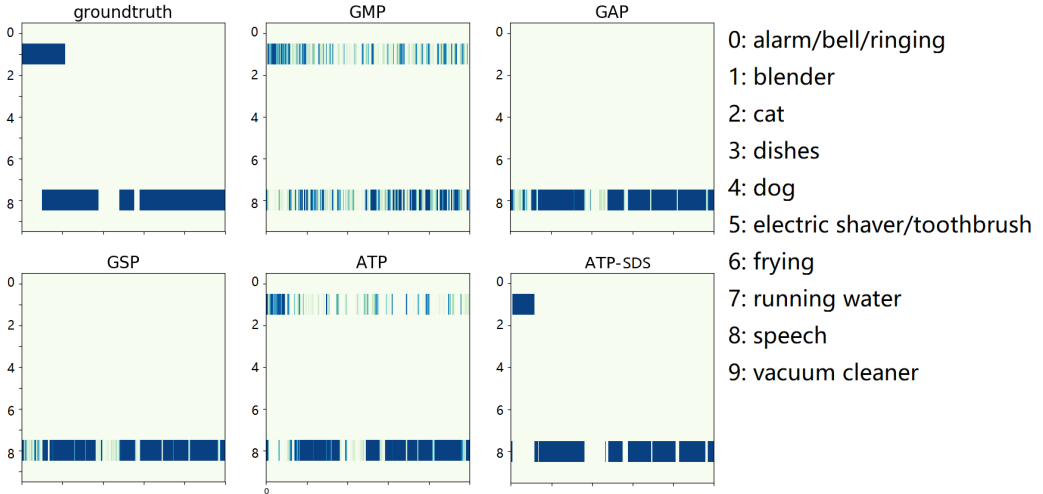


Fig. 10. Comparison of frame-level possibilities output with the groundtruth. The example is cherry-picked to indicate the points we highlight.

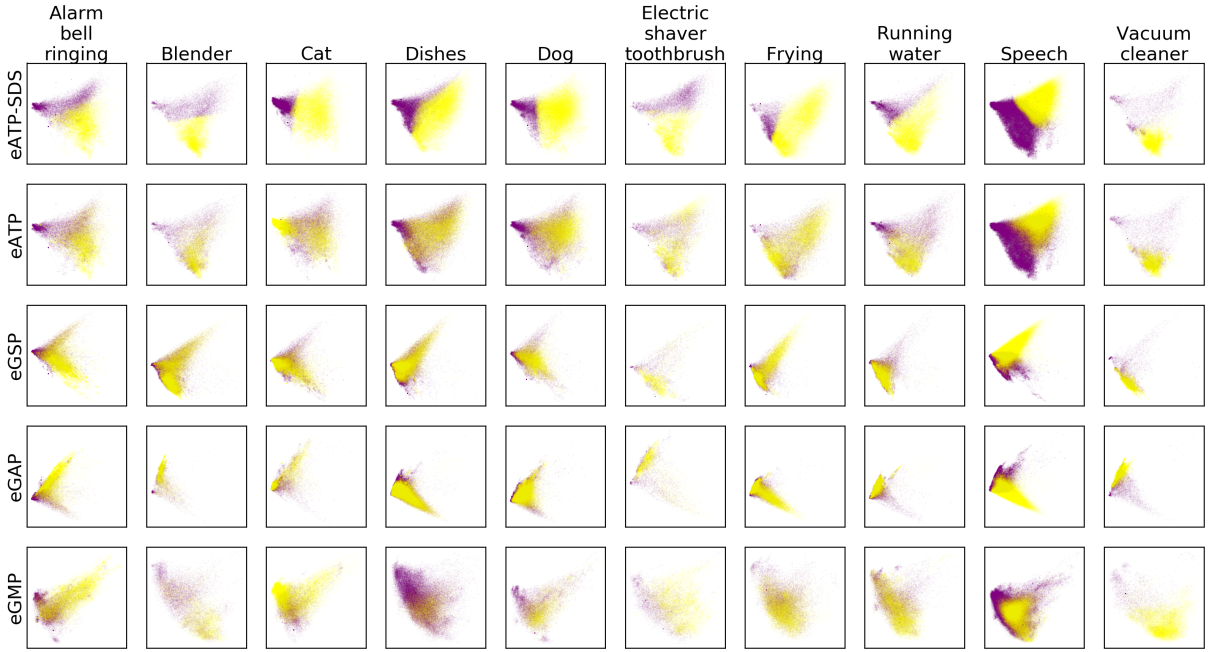


Fig. 11. The decision surfaces for different categories in the feature space generated from feature encoder (PCA).

find that the embedding-level models outperform the instance-level models, except that the event detection performance of the embedding-level ATP is a little worse than that of the instance-level ATP. The poor event detection performance might be due to the poor ability of the shared decision surface for the embedding-level ATP. Without taking account of SDS and DF, ATP is dominant in event detection. We note that the embedding-level GMP performs best on audio tagging but worst on event detection. The best clip-level performance attributes to the fact that the strategy which GMP takes to select frames to update tends to make fewer mistakes. The relative poor frame-level performance is due to the fact that such a strategy which updates limited frames once a time leads to weak predictions of those frames that are not critical to the clip-level decision making.

making.

As shown in Figure 10, we give an example audio clip of the test set to compare the frame-level performances of the 4 embedding-level models. Dark shadows in the figure represent frame-level probabilities output by the model without smoothing, the values of which range from 0 to 1. Compared with the groundtruth, GMP ignores those frames that are not critical to the clip-level decision making and make extremely discontinuous predictions both for “Blender” and “Speech”, while the strategies that GAP and GSP take to select frames pay more attention to negative frames, leading to an incorrect prediction for “Blender” but achieving better boundary detection for “Speech”. ATP achieves a better tradeoff between the two conditions above.

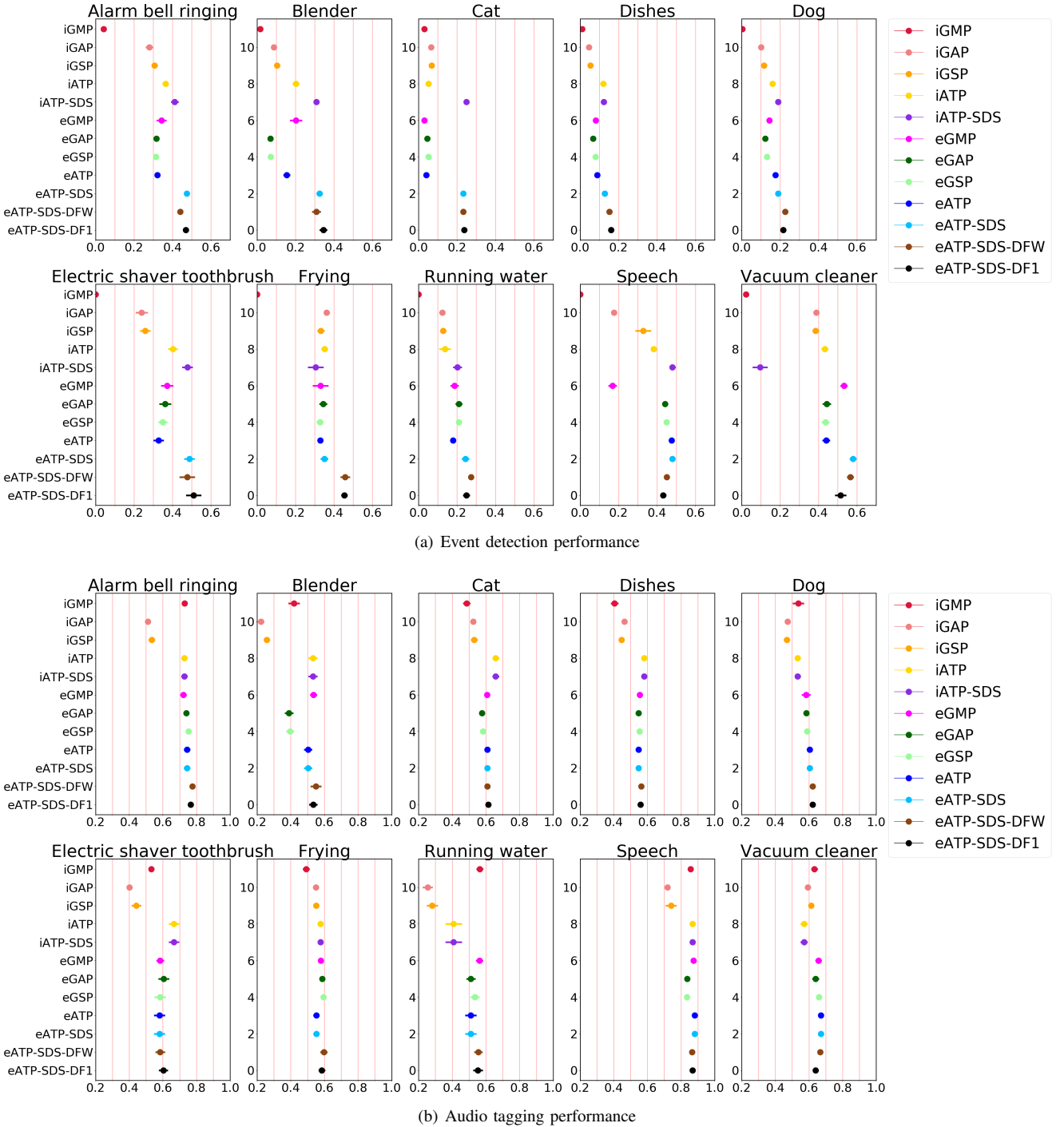


Fig. 12. The frame-level class-wise performance of models.

C. The effect of SDS on boundary detection

When we take SDS as decision surface for event detection, the frame-level average performance of the instance-level ATP is improved by 2.4 percentage points and that of the embedding-level ATP is improved by 9.6 percentage points as shown in Table II. As shown in Figure 10, we give an example audio clip of the test set to compare the frame-level performances of ATP and ATP-SDS. The predictions of ATP-SDS are obviously closer to groundtruths.

As shown in Figure 11, we transform the high-level feature

representations generated from the feature encoders of the embedding-level models into a two-dimensional space using principal components analysis (PCA) for observation. To highlight the frame-level decision surface, we only draw all the frames in positive clips (clips predicted to be positive). The yellow points represent frames predicted to be positive and purple points represent frames predicted to be negative. We can intuitively find that SDS clearly matches the boundary of two clusters discussed in Section IV-B. However, the shared decision surfaces of ATP, GSP, GAP and GMP show

a poor ability to separate these two clusters and lead to poor performance on event detection. Among them, the constraint that the shared decision surface of GSP is exactly consistent with its SDS hinders the flexible formation of SDS and exerts a negative effect on the separation of the two clusters. These observation exactly meets what we expect in Section IV-B.

It is worth mentioning that since the clear boundaries shown in Figure 11 separate the frames that predicted to be positive or negative rather than the groundtruths, the event detection performance is not as manifest as that of the separation of the two clusters.

D. The effect of DF on multi-label classification

When we combine embedding-level ATP-SDS with DF, the frame-level average performance of ATP-SDS with DFW outperforms ATP-SDS by 0.9 percentage points and that of ATP-SDS with DF1 outperforms ATP-SDS by 1 percentage points as shown in Table II. We report average frame-level F_1 and average clip-level F_1 of 20 experiments of all 10 event categories in Figure 12.

As shown in Figure 6, “Dishes” and “Frying” often occur in co-occurrence with each other and have a relatively small proportion in the training set while “Speech” often occurs in co-occurrence with any other categories. “Running water” also often occurs in co-occurrence with “Dishes”. As shown in Figure 12, ATP-SDS with DFW and DF1 did improve class-wise performances of “Dishes”, “Frying” and “Running water” both on event detection and audio tagging. This is because the separate subspaces of each category reduce the interference between them. However, the class-wise performance of ATP-SDS with DFW and DF1 for “Speech” is a little worse. We argue that since the number of clips containing “Speech” is much larger than that of clips containing any other event categories in the training set, the feature encoder without employing DF tends to form a high-level feature space more suitable for the event category “Speech”. When DF is employed, the other categories are much less disturbed by “Speech” and make a more balanced contribution to the feature encoder, which raises overall class-wise performances but also leads a little poorer performance of category “Speech”.

Another point is that DF reduces redundant weights of the model and improve performance while improving the training efficiency. Therefore, we argue that DF is a regularization method to deal with multi-label problems using the unbalanced dataset, which is worth pushing further.

VII. CONCLUSIONS

In this paper, we present how to generate frame-level probabilities for the embedding-level MIL approach and propose a specialized decision surface (SDS) and a disentangled feature (DF) for weakly-supervised polyphonic SED.

Firstly, we approach it as an MIL problem and then introduce an MIL framework with neural networks and pooling module. This framework is common in some weakly-supervised tasks and is grouped into two approaches: the instance-level approach and the embedding-level approach. We enable the embedding-level approach to make instance-level predictions and demonstrate the embedding-level approach tends to outperform the

instance-level approach on experimental dataset. Based on the exploration of the ability of the embedding-level approach to produce frame-level probabilities, we propose a specialized decision surface (SDS) to detect more accurate boundaries of events.

Secondly, to tackle the common problem causing by category co-occurrence between categories and data unbalance in the multi-label task, we propose a disentangled feature, which determines several certain subspaces for different categories without pre-training according to the prior information. In terms of optimizing the structure of the neural network, DF reduces redundant weights in the network and improves the training efficiency. From the perspective of feature space, DF optimizes the feature encoder and reduces the volume of high-level feature space of categories with insufficient samples, thus making it easier to learn more compact distribution. At the same time, DF, combined with prior information about co-occurrence between categories, reduces the interference between categories and improves the performance of the model.

Finally, the results of experiments on the dataset of DCASE2018 task 4 confirm our conjecture, which achieves a frame-level F_1 of 39.0%, outperforming the first place in the challenge by 6.6 percentage points.

ACKNOWLEDGMENT

This work is partly supported by Beijing Natural Science Foundation (4172058).

REFERENCES

- [1] J. P. Bello, C. Silva, O. Nov, R. L. DuBois, A. Arora, J. Salamon, C. Mydlarz, and H. Doraiswamy, “Sonyc: A system for the monitoring, analysis and mitigation of urban noise pollution,” *arXiv preprint arXiv:1805.00889*, 2018.
- [2] D. Stowell and D. Clayton, “Acoustic event detection for multiple overlapping similar sources,” in *2015 IEEE Workshop on Applications of Signal Processing to Audio and Acoustics (WASPAA)*. IEEE, 2015, pp. 1–5.
- [3] J. Salamon, J. P. Bello, A. Farnsworth, M. Robbins, S. Keen, H. Klinck, and S. Kelling, “Towards the automatic classification of avian flight calls for bioacoustic monitoring,” *PloS one*, vol. 11, no. 11, p. e0166866, 2016.
- [4] M. Crocco, M. Cristani, A. Trucco, and V. Murino, “Audio surveillance: A systematic review,” *ACM Computing Surveys (CSUR)*, vol. 48, no. 4, p. 52, 2016.
- [5] S. Goetze, J. Schroder, S. Gerlach, D. Hollosi, J.-E. Appell, and F. Wallhoff, “Acoustic monitoring and localization for social care,” *Journal of Computing Science and Engineering*, vol. 6, no. 1, pp. 40–50, 2012.
- [6] S. Hershey, S. Chaudhuri, D. P. Ellis, J. F. Gemmeke, A. Jansen, R. C. Moore, M. Plakal, D. Platt, R. A. Sauroos, B. Seybold *et al.*, “CNN architectures for large-scale audio classification,” in *2017 IEEE International Conference on Acoustics, Speech and Signal Processing (ICASSP)*. IEEE, 2017, pp. 131–135.
- [7] M. Oquab, L. Bottou, I. Laptev, and J. Sivic, “Is object localization for free? weakly-supervised learning with convolutional neural networks,” in *Proceedings of the IEEE Conference on Computer Vision and Pattern Recognition (CVPR)*, 2015, pp. 685–694.
- [8] B. Zhou, A. Khosla, A. Lapedriza, A. Oliva, and A. Torralba, “Learning deep features for discriminative localization,” in *Proceedings of the IEEE conference on computer vision and pattern recognition (CVPR)*, 2016, pp. 2921–2929.
- [9] A. Kolesnikov and C. H. Lampert, “Seed, expand and constrain: Three principles for weakly-supervised image segmentation,” in *European Conference on Computer Vision (ECCV)*. Springer, 2016, pp. 695–711.

- [10] Q. Kong, Y. Xu, W. Wang, and M. D. Plumbley, "A joint separation-classification model for sound event detection of weakly labelled data," in *2018 IEEE International Conference on Acoustics, Speech and Signal Processing (ICASSP)*. IEEE, 2018, pp. 321–325.
- [11] Y. Wang, J. Li, and F. Metze, "Comparing the max and noisy-or pooling functions in multiple instance learning for weakly supervised sequence learning tasks," *Proc. Interspeech 2018*, pp. 1339–1343, 2018.
- [12] M. Ilse, J. M. Tomczak, and M. Welling, "Attention-based deep multiple instance learning," *arXiv preprint arXiv:1802.04712*, 2018.
- [13] O. Maron and T. Lozano-Pérez, "A framework for multiple-instance learning," in *Advances in neural information processing systems*, 1998, pp. 570–576.
- [14] T. G. Dietterich, R. H. Lathrop, and T. Lozano-Pérez, "Solving the multiple instance problem with axis-parallel rectangles," *Artificial intelligence*, vol. 89, no. 1-2, pp. 31–71, 1997.
- [15] G. Quellec, G. Cazuguel, B. Cochener, and M. Lamard, "Multiple-instance learning for medical image and video analysis," *IEEE reviews in biomedical engineering*, vol. 10, pp. 213–234, 2017.
- [16] Y. Xu, T. Mo, Q. Feng, P. Zhong, M. Lai, I. Eric, and C. Chang, "Deep learning of feature representation with multiple instance learning for medical image analysis," in *2014 IEEE international conference on acoustics, speech and signal processing (ICASSP)*. IEEE, 2014, pp. 1626–1630.
- [17] G. Papandreou, L.-C. Chen, K. P. Murphy, and A. L. Yuille, "Weakly-and semi-supervised learning of a deep convolutional network for semantic image segmentation," in *Proceedings of the IEEE international conference on computer vision (ICCV)*, 2015, pp. 1742–1750.
- [18] J. Wu, Y. Zhao, J.-Y. Zhu, S. Luo, and Z. Tu, "Milcut: A sweeping line multiple instance learning paradigm for interactive image segmentation," in *Proceedings of the IEEE Conference on Computer Vision and Pattern Recognition (CVPR)*, 2014, pp. 256–263.
- [19] D. Pathak, E. Shelhamer, J. Long, and T. Darrell, "Fully convolutional multi-class multiple instance learning," *arXiv preprint arXiv:1412.7144*, 2014.
- [20] Z.-H. Zhou and M.-L. Zhang, "Neural networks for multi-instance learning," in *Proceedings of the International Conference on Intelligent Information Technology (ICCT), Beijing, China*, 2002, pp. 455–459.
- [21] J. Wu, Y. Yu, C. Huang, and K. Yu, "Deep multiple instance learning for image classification and auto-annotation," in *Proceedings of the IEEE Conference on Computer Vision and Pattern Recognition (CVPR)*, 2015, pp. 3460–3469.
- [22] O. Z. Kraus, J. L. Ba, and B. J. Frey, "Classifying and segmenting microscopy images with deep multiple instance learning," *Bioinformatics*, vol. 32, no. 12, pp. i52–i59, 2016.
- [23] T.-W. Su, J.-Y. Liu, and Y.-H. Yang, "Weakly-supervised audio event detection using event-specific gaussian filters and fully convolutional networks," in *2017 IEEE International Conference on Acoustics, Speech and Signal Processing (ICASSP)*. IEEE, 2017, pp. 791–795.
- [24] Q. Kong, Y. Xu, W. Wang, and M. D. Plumbley, "A joint detection-classification model for audio tagging of weakly labelled data," in *2017 IEEE International Conference on Acoustics, Speech and Signal Processing (ICASSP)*. IEEE, 2017, pp. 641–645.
- [25] A. Kumar, M. Khadkevich, and C. Fügen, "Knowledge transfer from weakly labeled audio using convolutional neural network for sound events and scenes," in *2018 IEEE International Conference on Acoustics, Speech and Signal Processing (ICASSP)*. IEEE, 2018, pp. 326–330.
- [26] Y. Xu, Q. Kong, W. Wang, and M. D. Plumbley, "Large-scale weakly supervised audio classification using gated convolutional neural network," in *2018 IEEE International Conference on Acoustics, Speech and Signal Processing (ICASSP)*. IEEE, 2018, pp. 121–125.
- [27] B. McFee, J. Salamon, and J. P. Bello, "Adaptive pooling operators for weakly labeled sound event detection," *IEEE/ACM Transactions on Audio, Speech and Language Processing (TASLP)*, vol. 26, no. 11, pp. 2180–2193, 2018.
- [28] Y. Wang, J. Li, and F. Metze, "A comparison of five multiple instance learning pooling functions for sound event detection with weak labeling," in *2019 IEEE International Conference on Acoustics, Speech and Signal Processing (ICASSP)*. IEEE, 2019, pp. 31–35.
- [29] E. Cakir, T. Heittola, H. Huttunen, and T. Virtanen, "Polyphonic sound event detection using multi label deep neural networks," in *2015 international joint conference on neural networks (IJCNN)*. IEEE, 2015, pp. 1–7.
- [30] G. Parascandolo, H. Huttunen, and T. Virtanen, "Recurrent neural networks for polyphonic sound event detection in real life recordings," in *2016 IEEE International Conference on Acoustics, Speech and Signal Processing (ICASSP)*. IEEE, 2016, pp. 6440–6444.
- [31] E. Cakir, G. Parascandolo, T. Heittola, H. Huttunen, and T. Virtanen, "Convolutional recurrent neural networks for polyphonic sound event detection," *IEEE/ACM Transactions on Audio, Speech, and Language Processing (TASLP)*, vol. 25, no. 6, pp. 1291–1303, 2017.
- [32] T. Hayashi, S. Watanabe, T. Toda, T. Hori, J. Le Roux, K. Takeda, T. Hayashi, S. Watanabe, T. Toda, T. Hori *et al.*, "Duration-controlled lstm for polyphonic sound event detection," *IEEE/ACM Transactions on Audio, Speech and Language Processing (TASLP)*, vol. 25, no. 11, pp. 2059–2070, 2017.
- [33] K. Imoto and S. Kyochi, "Sound event detection using graph laplacian regularization based on event co-occurrence," in *2019 IEEE International Conference on Acoustics, Speech and Signal Processing (ICASSP)*. IEEE, 2019, pp. 1–5.
- [34] J. Yan, Y. Song, W. Guo, L.-R. Dai, I. McLoughlin, and L. Chen, "A region based attention method for weakly supervised sound event detection and classification," in *2019 IEEE International Conference on Acoustics, Speech and Signal Processing (ICASSP)*. IEEE, 2019, pp. 755–759.
- [35] R. Serizel, N. Turpault, H. Eghbal-Zadeh, and A. Parag Shah, "Large-Scale Weakly Labeled Semi-Supervised Sound Event Detection in Domestic Environments," July 2018, submitted to DCASE2018 Workshop. [Online]. Available: <https://hal.inria.fr/hal-01850270>
- [36] J. F. Gemmeke, D. P. Ellis, D. Freedman, A. Jansen, W. Lawrence, R. C. Moore, M. Plakal, and M. Ritter, "Audio set: An ontology and human-labeled dataset for audio events," in *2017 IEEE International Conference on Acoustics, Speech and Signal Processing (ICASSP)*. IEEE, 2017, pp. 776–780.
- [37] S. Ioffe and C. Szegedy, "Batch normalization: Accelerating deep network training by reducing internal covariate shift," *arXiv preprint arXiv:1502.03167*, 2015.
- [38] Brian McFee, Colin Raffel, Dawen Liang, Daniel P.W. Ellis, Matt McVicar, Eric Battenberg, and Oriol Nieto, "librosa: Audio and Music Signal Analysis in Python," in *Proceedings of the 14th Python in Science Conference*, Kathryn Huff and James Bergstra, Eds., 2015, pp. 18 – 24.
- [39] L. JiaKai, "Mean teacher convolution system for dcase 2018 task 4," DCASE2018 Challenge, Tech. Rep., September 2018.
- [40] D. P. Kingma and J. Ba, "Adam: A method for stochastic optimization," *arXiv preprint arXiv:1412.6980*, 2014.
- [41] A. Mesaros, T. Heittola, and T. Virtanen, "Metrics for polyphonic sound event detection," *Applied Sciences*, vol. 6, no. 6, p. 162, 2016. [Online]. Available: <http://www.mdpi.com/2076-3417/6/6/162>



Liwei Lin received the B.E. degree in Computer Science and Technology from China Agricultural University, Beijing, China, in 2017. She is currently pursuing an M.E. degree in Computer Science and Technology in Institute of Computing Technology, Chinese Academy of Sciences, Beijing, China. her research interest includes audio signal processing and machine learning.



Xiangdong Wang is an associate professor in Institute of Computing Technology, Chinese Academy of Sciences, Beijing, China. He received Doctors degree in Computer Science at Institute of Computing Technology, Chinese Academy of Sciences, Beijing, China, in 2007. His research field includes human-computer interaction, speech recognition and audio processing.



Hong Liu is an associate professor in Institute of Computing Technology, Chinese Academy of Sciences, Beijing, China. She received her Doctors degree in Computer Science at Institute of Computing Technology, Chinese Academy of Sciences, Beijing, China, in 2007. Her research field includes human-computer interaction, multimedia technology, and video processing.



Yueliang Qian is a professor in Institute of Computing Technology, Chinese Academy of Sciences, Beijing, China. He received his Bachelors degree in Computer Science at Fudan University, Shanghai, China in 1983. His research field includes human-computer interaction and pervasive computing.